JACS
JOURNAL OF THE AMERICAN CHEMICAL SOCIETY
Article
pubs.acs.org/JACS

Axially Engineered Metal–Insulator Phase Transition by Graded Doping VO_2 Nanowires

Sangwook Lee,[†] Chun Cheng,[†] Hua Guo,[§] Kedar Hippalgaonkar,[‡] Kevin Wang,[†] Joonki Suh,[†] Kai Liu,[†,⊥] and Junqiao Wu*[,†,⊥]

[†]Department of Materials Science and Engineering and [‡]Department of Mechanical Engineering, University of California, Berkeley, California 94720, United States

[§]National Center for Electron Microscopy and [⊥]Division of Materials Sciences, Lawrence Berkeley National Laboratory, Berkeley, California 94720, United States

Supporting Information

ABSTRACT: The abrupt first-order metal–insulator phase transition in single-crystal vanadium dioxide nanowires (NWs) is engineered to be a gradual transition by axially grading the doping level of tungsten. We also demonstrate the potential of these NWs for thermal sensing and actuation applications. At room temperature, the graded-doped NWs show metal phase on the tips and insulator phase near the center of the NW, and the metal phase grows progressively toward the center when the temperature rises. As such, each individual NW acts as a micro-thermometer that can be simply read out with an optical microscope. The NW resistance decreases gradually with the temperature rise, eventually reaching 2 orders of magnitude drop, in stark contrast to the abrupt resistance change in undoped VO_2 wires. This novel phase transition yields an extremely high temperature coefficient of resistivity ~10%/K, simultaneously with a very low resistivity down to 0.001 Ω·cm, making these NWs promising infrared sensing materials for uncooled microbolometers. Lastly, they form bimorph thermal actuators that bend with an unusually high curvature, ~900 $m^{-1}\cdot K^{-1}$ over a wide temperature range (35–80 °C), significantly broadening the response temperature range of previous VO_2 bimorph actuators. Given that the phase transition responds to a diverse range of stimuli—heat, electric current, strain, focused light, and electric field—the graded-doped NWs may find wide applications in thermo-opto-electro-mechanical sensing and energy conversion.

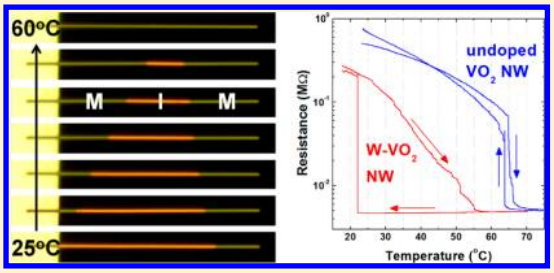

INTRODUCTION

Vanadium dioxide, a textbook example of strongly correlated electron material, is extremely interesting for exploration of condensed matter physics as well as various device applications. It undergoes a coupled structural–electronic phase transition from a monoclinic, insulating phase (I) at low temperatures to a rutile, metallic phase (M) at high temperatures.[1,2] The metal–insulator transition (MIT) and structural transition occur concurrently at T_{MIT} = 67 °C. Across the MIT, VO_2 exhibits a drastic change in optical transparency, several orders of magnitude drop in resistivity, and a specimen size change up to 1%.[3−6] Exploiting these unique characteristics, a number of applications have been proposed or demonstrated, such as optical switch,[7] smart window coating,[8] Mott transistor,[9] memristor,[10] strain sensor,[11] gas sensor,[12] temperature sensor,[13] and thermal actuator.[14]

For all these applications, the functionality is within a very narrow temperature window around T_{MIT}, because the phase transition is first-order and occurs abruptly only near T_{MIT} = 67 °C. For many applications, it is necessary to tailor T_{MIT} to meet different needs. Doping of transition metal into VO_2 is widely used to tune the T_{MIT}. T_{MIT} can be decreased or increased depending on the oxidation state of the dopant; substitution of V^{4+} with W^{6+}, Mo^{6+}, and Nb^{5+} lowers the T_{MIT},[15−22] whereas Cr^{3+}, Ga^{3+}, and Al^{3+} raise it.[22−24] Among them, tungsten is known as the most effective dopant, enabling precise and wide-range control of T_{MIT}, reported with a nearly linear reduction rate of 18.4 °C/at.% for single-crystal VO_2 nanowires (NWs),[15] 24 °C/at.% for polycrystal thin films,[16] and 25–26 °C/at.% for powder and bulk single crystals.[17,18] However, in all these cases, the W-doping of VO_2 is spatially homogeneous; therefore, it simply shifts T_{MIT} to another value and does not modify the abrupt first-order nature of the MIT. The response temperature is still limited to a very narrow window around the new T_{MIT}, and a wide temperature responsivity is lacking.

In this work, we lift this limit by engineering a spatially graded MIT along individual single-crystal VO_2 NWs. The VO_2 NWs are axially graded-doped with W, forming $W_xV_{1-x}O_2$ NWs where x varies continuously along the NW axis, thus achieving a NW system that supports a MIT responding to a wide range of activation temperatures, practically analogous to a second-order phase transition. The M and I domains evolve gradually along the NW axis, leading to unique characteristics absent in undoped VO_2: gradual but exceedingly large total changes in optical contrast, electrical resistivity, and NW length.

Received: January 24, 2013
Published: March 6, 2013

dx.doi.org/10.1021/ja400658u | J. Am. Chem. Soc. 2013, 135, 4850–4855

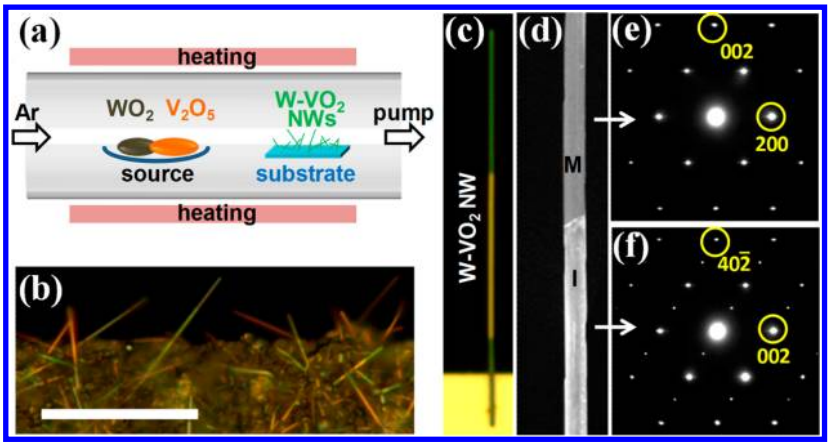

Figure 1. (a) Schematic of growing the graded-doped $W_xV_{1-x}O_2$ NWs. (b) Optical image of an as-grown sample at room temperature (scale bar, 20 μm). (c,d) Optical (c) and TEM (d) images of a typical graded-doped $W_xV_{1-x}O_2$ NW (length ~32 μm, width ~210 nm). The NW was transferred onto a Si substrate from the as-grown substrate. Optical images were taken using unpolarized white light. Visual color of the NW is a combined result of multiple factors including illumination light spectrum and resolution limit of the optics. (e,f) Electron diffraction pattern taken from the dark green region (e) and bright yellow region (f). The patterns are indexed to rutile (metallic phase, M) and monoclinic (insulating phase, I) structure of VO_2, using rutile-[010] and monoclinic-[010] zone axes, respectively.

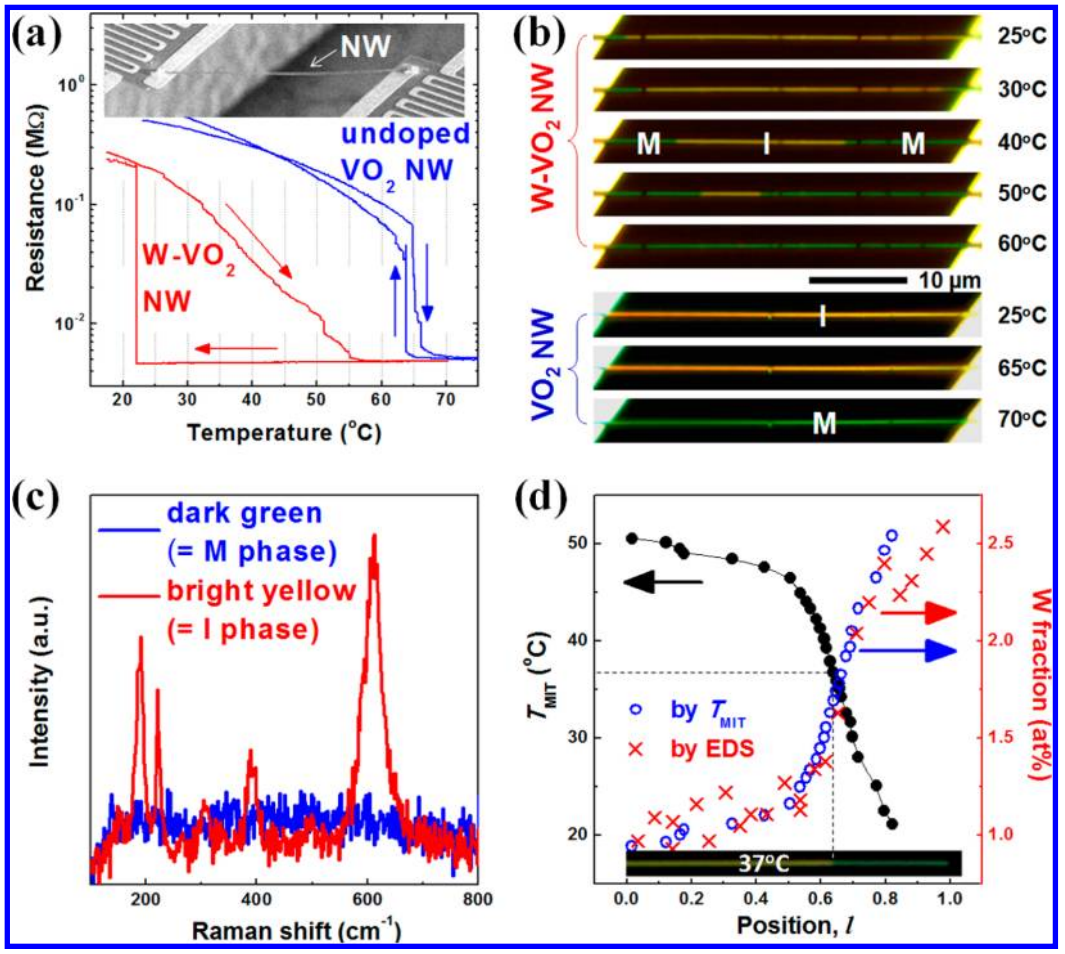

Figure 2. (a) Temperature dependence of resistance of a graded-doped $W_xV_{1-x}O_2$ NW and an undoped VO_2 NW. The resistance was measured on suspended pads (inset) to minimize strain. (b) Optical images of the graded-doped $W_xV_{1-x}O_2$ NW device (upper panel) and the undoped VO_2 NW device (lower panel) at various temperatures during heating. (c) Raman spectra taken from the dark part and the bright part of the graded-doped $W_xV_{1-x}O_2$ NW. The peaks for the bright part are identified as I phase of VO_2 (monoclinic). There are no peaks related to other stoichiometries of vanadium oxides. (d) Local MIT temperature (left axis) and W fraction (right axis). The latter was measured by EDS and calculated from the measured T_{MIT}, respectively. The horizontal axis is positioned along the graded-doped NW from the center (l = 0) to the tip (l = 1). l = 1 corresponds to 20 μm. The inset shows an optical image of the analyzed NW at 37 °C as an example.

dx.doi.org/10.1021/ja400658u | J. Am. Chem. Soc. 2013, 135, 4850−4855

Enabled by these characteristics, we propose or demonstrate novel applications as an optically readable microthermometer, uncooled infrared bolometer, and bimorph thermal microactuator.

RESULTS AND DISCUSSION

The graded-doped $W_xV_{1-x}O_2$ NWs were grown by the vapor transport method as schematically shown in Figure 1a, similar to a previous growth method for high-density undoped VO_2 wires,[25] except that WO_2 powder was added as W-doping source. Downstream, NWs were produced on an unpolished quartz substrate, as shown in Figure 1b. The as-synthesized NWs free stand randomly on the substrate, and the lengths are in the range of 5−50 μm. Figure 1c shows optical image of a typical NW (length ∼32 μm, width ∼210 nm) cantilevered from the edge of a substrate. Most notably, at room temperature, the M and I phases coexist axially within the single NW. It is well known that these two phases are clearly distinguishable by their optical reflection under white light illumination: the dark domain (dark green in this work) is the M phase, and the bright domain (bright yellow in this work) is the I phase.[4] Almost all NWs have three distinctive domains: M phase at both tips and I phase in the middle part. These phases were cross-checked by transmission electron microscopy (TEM). The selected area electron diffraction (SAED) pattern of the NW (Figure 1e,f) shows that the dark green part is indeed M phase (rutile, $P4_2/mnm$), while the bright yellow part is I phase (monoclinic, $P2_1/c$). The single-crystallinity of the NW is confirmed by the fact that the SAED pattern does not vary when taken at different spots along the NW axis. Therefore, it is clear that the tips of the NWs are W-doped more heavily than the middle part, such that the T_{MIT} at the tips is below room temperature, while at the middle part it is above room temperature.

In the optical and TEM imaging above, the NW is free-standing. This is important in order to probe the intrinsic phase transition and domain structure. It has been shown that, under strain, the MIT temperature and the M-I domain structure of VO_2 appear different from those of free-standing VO_2.[3,4] A free-standing VO_2 NW or a free-standing uniformly W-doped VO_2 NW undergoes the MIT abruptly when temperature is raised across its T_{MIT}.[3,15] However, when the same NW is assembled into a two-probe device where the two ends (and only the two ends) are firmly clamped on a rigid substrate by electrodes, the M phase grows gradually along the NW as a function of temperature.[26] This is because this is the minimum-energy M-I domain structure of the NW when an additional elastic energy term is introduced by strain accumulated in such an end-end clamped configuration.[26,27] Therefore, externally imposed strain should be avoided when the intrinsic MIT behavior is to be characterized.

To eliminate strain accumulation in measuring the electrical resistance of these NWs, we use the suspended microdevice pads typically used for isolated thermal transport measurements;[28] here the pads are conductive and suspended by long flexural arms, serving as two electrical contacts to the NW. Unlike ordinary NW devices firmly clamped on solid substrates, however, in our case the suspended pads are free to move, and thus the NW is free to shrink or elongate to avoid axial strain accumulation. A single NW was transferred to bridge the two pads (Figure 2a, inset), and Pt was deposited to bond the NW onto the pads using a focused ion beam (see Figure S1, Supporting Information). A number of $W_xV_{1-x}O_2$ and undoped VO_2 devices (number >5) were fabricated in this way. The typical length and width of NWs are ∼40 μm and ∼300 nm, respectively. All devices showed linear $I-V$ curves, indicating ohmic contacts. Figure 2a plots a typical resistance−temperature curve of a graded-doped $W_xV_{1-x}O_2$ NW and an undoped VO_2 NW. Here the temperature ramping rate is controlled to be very slow (<2.5 °C/min), to eliminate kinetic effects. The undoped VO_2 NW shows an expected[3] sharp resistance switching around 67 °C with a ∼2 °C hysteresis. We note that the T_{MIT} may be also affected by chemical non-stoichiometry of the NW.[29] In stark contrast, resistance of the graded-doped $W_xV_{1-x}O_2$ NW decreases gradually from room temperature to 60 °C without the abrupt resistance switching. This resistance behavior results in an exceedingly large temperature coefficient of resistivity (TCR) of $-(12 \pm 2)$%/K. The TCR is defined as $(1/\rho)(d\rho/dT) = d(\ln \rho)/dT)$, where ρ is resistivity. The TCR is a key parameter for many thermal sensing applications, such as electrical thermometers and infrared bolometers (see below).

The origin of this gradual MIT that lasts over a ΔT = 30 °C can be understood from the concurrently taken optical images of the graded-doped NW. As shown in Figure 2b, with the increase in temperature, the M phase grows out of the two ends of the NW, followed by a progressive invasion into the I phase toward the middle of the NW, and the entire NW turns into a single M phase at 55−60 °C. Such a domain behavior was observed from all graded W-doped VO_2 NWs, but not from the undoped VO_2 NWs. Moreover, even when the NW was cantilevered at one end from the edge of a heated substrate, the M phase grew from both the root and the tip of the NW (Figure S2, Supporting Information). Therefore, we rule out the possibility that temperature gradient along the NW axis might cause this domain behavior. The axially progressed M-I domain wall means that the local T_{MIT} itself is encoded by the growth, and varies gradually along the axis, from heavily W-doped tips to a lightly W-doped center. The coexisting M and I phases along a single NW is further confirmed by their micro-Raman spectra in Figure 2c. Figure 2d shows axially varying T_{MIT} from the center (position l = 0) to one of the tips (l = 1) of a graded-doped $W_xV_{1-x}O_2$ NW, and the W-doping fraction measured along the NW axis by energy dispersive X-ray spectroscopy (EDS). The EDS results verify that the NW is graded W-doped and the doping level increases from 1.0 at.% at l = 0 to 2.6 at.% at l = 1. The measured W-doping level agrees well with the predicted W fraction (also plotted in Figure 2d), converted from the measured T_{MIT} using the T_{MIT} reduction rate, −18.4 °C/at.% of W, reported from homogeneously W-doped VO_2 NWs.[15] We note that when the graded-doped $W_xV_{1-x}O_2$ NWs are cooled from high temperatures where the NW is in full M state, they always show a large hysteresis as in Figure 2a. On the other hand, when they are cooled from an M-I-M domain configuration at intermediate temperatures, they show only a small (<5 °C) hysteresis followed by a gradual transition back to the full I state. This is an effect of large supercooling because of the lack of nucleation site for the transition starting from the full M state. As shown in our previous work,[30] the M-I domain wall or twin walls in VO_2 can serve as sites to seed the growth of new phase, thus eliminate superheating or supercooling during the MIT. However, when the NW is fully in the M state, an M-I wall is absent, and the tetragonal crystal structure of the M-phase also precludes the possibility of structural twining. Therefore the system has to undergo a large supercooling before the first I domain appears.

dx.doi.org/10.1021/ja400658u | J. Am. Chem. Soc. 2013, 135, 4850−4855

This is not the case for the transition starting from an M-I-M state where the M-I domain wall acts as the seed for growth of new phase. Therefore, a large kinetic asymmetry with a strong supercooling is seen in the MIT of these NWs.

Due to the stark color contrast between the M and I domains, the M-I domain wall can be easily resolved with an optical microscope. Its axial progress with temperature rise naturally offers a single-NW microthermometer that can be optically read out. Optically readable microthermometers have been demonstrated utilizing temperature-sensitive light emission of quantum dots[31] or molecules.[32] However, in those cases an excitation light source and a spectrometer are needed to record and spectrally resolve the emitted light. In our case by a rapid, simple optical imaging of the M-I domain wall position along the NW, local temperature can be determined after proper calibration. Moreover, the temperature range over which the NW thermometer works is between room temperature and ~60 °C, a temperature range of special importance in biology and microfluidics. We note that an undoped VO_2 NW can also support an axially gradual MIT when it is firmly clamped at its two ends on a rigid substrate.[26] However, the requirement of end clamping is undesired for application, while in our case this is achieved with W-doping.

Now we turn to another potential application, infrared detection. For electromagnetic radiation in the far-infrared spectral range, conventional p-n junction based photodetectors do not work because the infrared light energy is below their bandgap. In this case bolometers are typically used, which measure the incident infrared light intensity by monitoring the resistance (R) change of an infrared-sensing material. The material absorbs the infrared light and heats up, thus lowering its R. Typical bolometers are cooled by liquid helium to reduce optical and electrical noises, which add undesired cost, volume and weight. For uncooled bolometers, high performance requires the following properties from the sensing material: (1) strong infrared absorption to maximize efficiency, (2) a high TCR for maximum sensitivity, and (3) a low resistivity (ρ) to minimize thermal noise and Joule heating. Achieving a high TCR and simultaneously low ρ is a challenge for semiconductors because they are mutually exclusive: $\rho = \rho_0 \exp(E_a/k_BT)$, and TCR = $(1/\rho)(d\rho/dT) = -E_a/k_BT^2$, where E_a is the thermal activation energy of ρ. Therefore, a high TCR typically correlates with a high ρ.

VO_2 thin films have a relatively high TCR of 2−5%/K in the I phase, but their high ρ of 0.1−1 Ω·cm makes them unsuitable for uncooled bolometer application.[33,34] Moreover, their abrupt, first-order MIT is considered as a nuisance that needs to be avoided, because it introduces high nonlinearity in the sensing response. Other vanadium oxide (VO_x) thin films with various stoichiometries free of MIT have been used as commercial bolometer sensing material, taking advantage of their strong infrared absorption, relatively high TCR (2−3%/K) and low ρ (0.05−0.1 Ω·cm).[33,34] Our graded W-doped VO_2 offers a new, superior bolometer material by exploiting the MIT, as opposed to avoiding it. First of all, VO_2 and W-doped VO_2 are intrinsically strongly absorptive in the far-infrared region, especially in the M phase.[35,36] Figure 3 plot the TCR and ρ of the graded-doped $W_xV_{1-x}O_2$ NWs compared to VO_x thin films that are currently used as the working material for uncooled bolometers. The graded-doped $W_xV_{1-x}O_2$ NWs exhibit an exceptionally high TCR on the order of 10%/K, together with a low ρ between 0.001 and 0.1 Ω·cm. These two parameters are superior to VO_2 thin films,[33,34,37,38] VO_x thin films,[33,34,39−41] $W_xV_{1-x}O_2$ (x = 0.015) thin films,[20] and undoped VO_2 NW. Therefore, the spatial progressing MIT of graded W-doped VO_2 presents a new candidate for prospective bolometer material by offering ~5 times higher TCR simultaneously with a lower ρ than commercially used bolometer materials. Compared to polycrystal VO_x thin films, the graded-doped single-crystal $W_xV_{1-x}O_2$ may have other advantages: (1) possibly low $1/f$ noise (another main factor affecting device sensitivity) because of its single-crystallinity and thus much fewer domain/grain boundaries;[42] and (ii) high effective infrared absorption due to the existence of the M phase with an absorption coefficient 5−100 times higher than that of the I phase in the infrared range of wavelength > ~ 8 μm.[43,44]

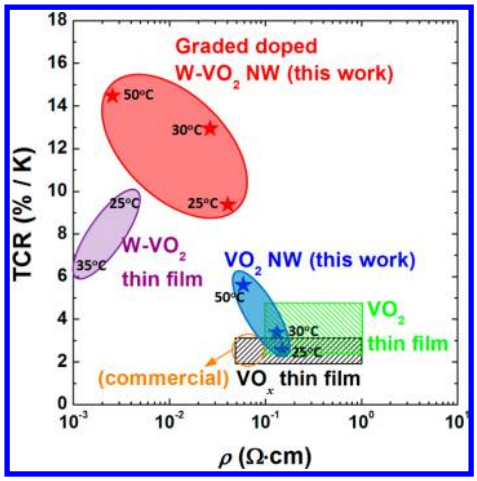

Figure 3. Temperature coefficient of resistivity versus resistivity of various sensing materials for uncooled infrared bolometer. The graded-doped $W_xV_{1-x}O_2$ NW is compared with VO_x thin films (refs 33, 34, 39−41), VO_2 thin films (refs 33, 34, 37, 38), W-doped VO_2 (1.5 at.%) thin film (ref 20), and VO_2 NW (this work). The stars are the data points measured in this work. An ideal bolometer material prefers high TCR and low ρ.

The axially engineered MIT in the graded-doped $W_xV_{1-x}O_2$ NWs also provides a means for constructing broad-range thermal microactuators. It is known that accompanying the MIT in VO_2, the structural phase transition introduces a spontaneous strain, $\varepsilon \approx 1\%$, along the rutile c-axis (c_R).[2] In NWs where the wire axis is always along c_R, the strain causes an abrupt shrinkage of the NW length by 1%. This effect has recently been used for thermal microactuators, in which a VO_2 NW is mechanically coupled with an inactive layer forming a bimorph. Crossing the MIT, the bimorph bends to high curvatures (κ), and outputs actuation at high force, high amplitude, and high speed compared to conventional actuators.[14,45−47] This phase transition-based actuation, however, is triggered abruptly near the VO_2 MIT temperature, ~67 °C, and does not respond to lower driving temperatures, which limits the operation responsivity, as shown in Figure 4. We found that W-doping retains the 1% spontaneous strain in VO_2 (Figure S3, Supporting Information), yet the NW length shrinkage occurs gradually instead of abruptly. This property offers a way to lower the temperature threshold and broaden the response range of undoped VO_2 actuators. Figure 4 shows the temperature-dependent κ change of a bimorph actuator comprised of a graded-doped $W_xV_{1-x}O_2$ NW coupled to a Cr overlayer as shown in the inset. The length and thickness of the NW are ~24 μm and ~250 nm, respectively. We coated ~90

dx.doi.org/10.1021/ja400658u | J. Am. Chem. Soc. 2013, 135, 4850−4855

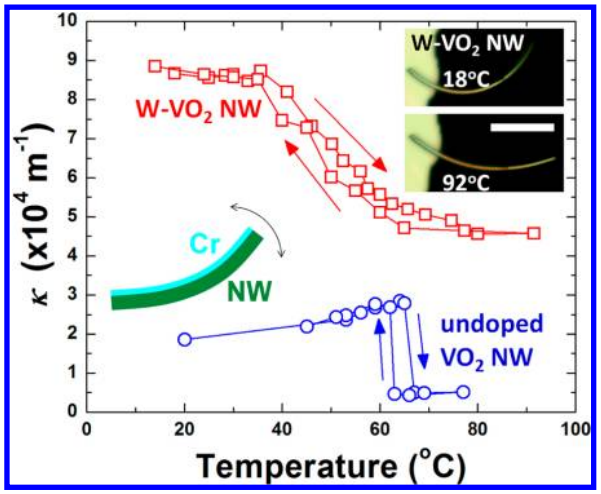

Figure 4. Temperature dependence of bending curvature of two bimorph thermal actuators, Cr on a graded-doped $W_xV_{1-x}O_2$ NW, and Cr on an undoped VO_2 NW. Upper inset shows optical images of the $W_xV_{1-x}O_2$-based actuator (scale bar, 10 μm) at 18 and 92 °C, and lower inset shows a scheme of the bimorph structure.

nm of Cr onto one side of the NW, because the maximum curvature change ($\Delta\kappa$) of a Cr/VO_2 bimorph is expected at a thickness ratio of ~0.37.[45] In contrast to the Cr/VO_2 bimorph, the κ of the Cr/$W_xV_{1-x}O_2$ changes gradually over a temperature range of 35−80 °C, with a rate $\Delta\kappa/\Delta T \approx 900$ $m^{-1}\cdot K^{-1}$, leading to an overall $\Delta\kappa \approx 4 \times 10^4$ m^{-1}. This wider range of working temperature, gradual κ change, and smaller $\Delta\kappa/dT$ (compared to Cr/VO_2 bimorph) allow precise control of the actuation displacement, while outputting large amplitude of the displacement. Moreover, it has been shown[14] that VO_2 provides a high volumetric work density ($Y\varepsilon^2/2$, where $Y = 140$ GPa is the Young's modulus) up to 7 J/cm^3. This allows the Cr/VO_2 bimorph actuator to deliver simultaneously high force and large amplitude in actuation. This work density is comparable to shape memory alloys, more than 10 times higher than that of most organic materials and electrostrictive polymers, hundreds of times higher than that of piezoelectric materials, and 3 orders of magnitude higher than that of human muscles.[48]

CONCLUSION

In summary, we synthesized W-doped VO_2 NWs where the doping level is axially graded from the two tips toward the center of the NW. These $W_xV_{1-x}O_2$ NWs exhibit axially graded metal−insulator phase transition and structural transition. Their extremely high temperature coefficient of resistivity, combined with the low resistivity, make them good candidates for far-infrared sensing material in uncooled bolometers; the high optical contrast between the two phases renders each individual NW an optically readable microthermometer; the gradual structural transition allows to form bimorph microactuators with high amplitude and wide temperature responsivity. We note that the coupled structural−electronic phase transition of VO_2 and $W_xV_{1-x}O_2$ can be activated by a diverse range of external stimuli: heat, electric current,[15] strain,[3] focused light,[14] and electrical field.[49,50] Consequently, the graded-doped $W_xV_{1-x}O_2$ NWs may find extensive applications in microscale thermo-opto-electro-mechanical signal transduction and energy conversion.

EXPERIMENTAL SECTION

Growth and Characterization of Graded-Doped $W_xV_{1-x}O_2$ NWs. The graded-doped $W_xV_{1-x}O_2$ NWs were synthesized using a vapor transport scheme modified from a previously reported method.[25] V_2O_5 and 20 wt% of WO_2 powder were placed in a quartz boat in the center of a horizontal tube furnace, and evaporated at 880 °C for 10 min, with Ar as the carrier gas (6.8 sccm) at 4 Torr of pressure. The reaction product was collected at 850 °C on an unpolished quartz substrate from downstream of the evaporated sources. The mechanism of axially graded doping of W in the VO_2 NWs is not yet fully understood, but a tentative explanation is given in the Supporting Information. The morphology, crystal structure, crystal orientation, and doping level of these NWs were characterized by optical microscopy, SEM, TEM, Raman spectroscopy, and EDS in TEM.

Fabrication and Characterization of NW-Based Devices. In order to measure the electrical property free of strain accumulation, we used suspended, flexural micropads to make electrical devices. Electrically conductive Pt lines were coated on the suspended pads and arms. An individual as-grown NW was transferred between two suspended, parallel pads, and Pt was deposited onto both ends of the NW using focused ion beam for good electrical contact with the pads. To make Cr/NW bimorph microactuators, Cr layers were deposited onto one side of graded-doped $W_xV_{1-x}O_2$ NWs by electron-beam evaporation with a deposition rate of 0.2 nm/s. The microactuators always bend toward Cr layer due to built-in stress between the Cr and the NW during the Cr evaporation. The sample temperature was controlled by global heating/cooling of the entire device with a ramping rate of 2.5 °C/min, using an electrical microheater combined with a resistive temperature sensor.

ASSOCIATED CONTENT

Supporting Information

Suspended pad device for electrical measurements, NW domain configuration at increasing temperatures, NW length change over the phase transition, and proposed growth mechanism. This material is available free of charge via the Internet at http://pubs.acs.org.

AUTHOR INFORMATION

Corresponding Author

wuj@berkeley.edu

Notes

The authors declare no competing financial interest.

ACKNOWLEDGMENTS

This work was supported by the National Science Foundation under Grant No. ECCS-1101779.

REFERENCES

(1) Eyert, V. *Ann. Phys.* **2002**, *11*, 650.
(2) Marezio, M.; McWhan, B.; Dernier, P. D.; Remeika, J. P. *Phys. Rev. B* **1972**, *5*, 2541.
(3) Cao, J.; Ertekin, E.; Srinivasan, V.; Fan, W.; Huang, S.; Zheng, H.; Yim, J. W. L.; Khanal, D. R.; Ogletree, D. F.; Grossman, J. C.; Wu, J. *Nat. Nanotechnol.* **2009**, *4*, 732.
(4) Wu, J.; Gu, Q.; Guiton, B. S.; de Leon, N. P.; Ouyang, L.; Park, H. *Nano Lett.* **2006**, *6*, 2313.
(5) Berglund, C. N.; Guggenheim, H. *J. Phys. Rev.* **1969**, *185*, 1022.
(6) Goodenough, J. B. *J. Solid State Chem.* **1971**, *3*, 490.
(7) Chain, E. E. *Appl. Opt.* **1991**, *30*, 2782.
(8) Gao, Y. F.; Wang, S. B.; Kang, L. T.; Chen, Z.; Du, J.; Liu, X. L.; Luo, H. J.; Kanehira, M. *Energy Environ. Sci.* **2012**, *5*, 8234.
(9) Hormoz, S.; Ramanathan, S. *Solid-State Electron.* **2010**, *54*, 654.
(10) Coy, H.; Cabrera, R.; Sepúlveda, N.; Fernández, F. E. *J. Appl. Phys.* **2010**, *108*, 113115.

(11) Hu, B.; Zhang, Y.; Chen, W.; Xu, C.; Wang, Z. L. *Adv. Mater.* **2011**, *23*, 3536.
(12) Strelcov, E.; Lilach, Y.; Kolmakov, A. *Nano Lett.* **2009**, *9*, 2322.
(13) Kim, B.-J.; Lee, Y. W.; Chae, B.-G.; Yun, S. J.; Oh, S.-Y.; Kim, H.-T.; Lim, Y.-S. *Appl. Phys. Lett.* **2007**, *90*, 023515.
(14) Liu, K.; Cheng, C.; Cheng, Z. T.; Wang, K.; Ramesh, R.; Wu, J. *Nano Lett.* **2012**, *12*, 6302.
(15) Gu, Q.; Falk, A.; Wu, J.; Ouyang, L.; Park, H. *Nano Lett.* **2007**, *7*, 363.
(16) Jin, P.; Nakao, S.; Tanemura, S. *Thin Solid Films* **1998**, *324*, 151.
(17) Rakotoniaina, J. C.; Mokrani-Tamellin, R.; Gavarri, J. R.; Vacquier, G.; Casalot, A.; Calvarin, G. *J. Solid State Chem.* **1993**, *103*, 81.
(18) Hörlin, T.; Niklewski, T.; Nygren, M. *Mater. Res. Bull.* **1972**, *7*, 1515.
(19) Whittaker, L.; Wu, T.-L.; Stabile, A.; Sambandamurthy, G.; Banerjeej, S. *ACS Nano* **2011**, *5*, 8861.
(20) Takami, H.; Kawatani, K.; Kanki, T.; Tanaka, H. *Jpn. J. Appl. Phys.* **2011**, *50*, 055804.
(21) Wu, Z. P.; Miyashita, A.; Yamamoto, S.; Abe, H.; Nashiyama, I.; Narumi, K.; Naramoto, H. *J. Appl. Phys.* **1999**, *86*, 5311.
(22) Fisher, B. *Phys. Chem. Solids* **1982**, *43*, 205.
(23) Brückner, W.; Gerlach, U.; Moldenhauer, W.; Brückner, H. P.; Mattern, N.; Oppermann, H.; Wolf, E. *Phys. Status Solidi A* **1976**, *38*, 93.
(24) Strelcov, E.; Tselev, A.; Ivanov, I.; Budai, J. D.; Zhang, J.; Tischler, J. Z.; Kravchenko, I.; Kalinin, S. V.; Kolmakov, A. *Nano Lett.* **2012**, *12*, 6198.
(25) Cheng, C.; Liu, K.; Xiang, B.; Suh, J.; Wu, J. *Appl. Phys. Lett.* **2012**, *100*, 103111.
(26) Wei, J.; Wang, Z. H.; Chen, W.; Cobden, D. H. *Nat. Nanotechnol.* **2009**, *4*, 420.
(27) Tselev, A.; Meunier, V.; Strelcov, E.; Shelton, W. A.; Luk'yanchuk, I. A.; Jones, K.; Proksch, R.; Kolmakov, A.; Kalinin, S. V. *ACS Nano* **2010**, *4*, 4412.
(28) Kim, P.; Shi, L.; Majumdar, A.; McEuen, P. L. *Phys. Rev. Lett.* **2001**, *87*, 215502.
(29) Zhang, S.; Kim, I. S.; Lauhon, L. *J. Nano Lett.* **2011**, *11*, 1443.
(30) Fan, W.; Cao, J.; Seidel, J.; Gu, Y.; Yim, J. W.; Barrett, C.; Yu, K. M.; Ji, J.; Ramesh, R.; Chen, L. Q.; Wu, J. *Phys. Rev. B* **2011**, *83*, 235102.
(31) Li, S.; Zhang, K.; Yang, J.-M.; Lin, L. W.; Yang, H. *Nano Lett.* **2007**, *7*, 3102.
(32) Wienken, C. J.; Baaske, P.; Rothbauer, U.; Braun, D.; Duhr, S. *Nat. Commun.* **2010**, *1*, 100.
(33) Gurvitch, M.; Luryi, S.; Polyakov, A.; Shabalov, A. *J. Appl. Phys.* **2009**, *106*, 104504.
(34) Niklaus, F.; Vieider, C.; Jakobsen, H. *Proc. SPIE* **2007**, *6836*, 68360D-1.
(35) Fu, D.; Liu, K.; Tao, T.; Lo, K.; Cheng, C.; Liu, B.; Zhang, R.; Bechtel, H. A.; Wu, J. *J. Appl. Phys.* **2013**, *113*, 043707.
(36) Soltani, M.; Chaker, M.; Haddad, E.; Kruzelecky, R.; Margot, J. *J. Vac. Sci. Technol. A* **2007**, *25*, 971.
(37) Cheng, Q.; Paradis, S.; Bui, T.; Almasri, M. *IEEE Sens. J.* **2011**, *11*, 167.
(38) Gurvitch, M.; Luryi, S.; Polyakov, A.; Shabalov, A.; Dudley, M.; Wang, G.; Ge, S.; Yakovlev, V. *J. Appl. Phys.* **2007**, *102*, 033504.
(39) Kang, H. K.; Han, Y. H.; Shin, H. J.; Moon, S.; Kim, T. H. *J. Vac. Sci. Technol. B* **2003**, *21*, 1027.
(40) Wang, B.; Lai, J. J.; Zhao, E. J.; Hu, H. M.; Liu, Q.; Chen, S. H. *Opt. Eng.* **2012**, *51*, 074003.
(41) Radford, W.; Murphy, D.; Ray, M.; Propst, S.; Kennedy, A.; Kojiro, J.; Woolaway, J.; Soch, K. *Proc. SPIE* **1996**, *2746*, 88.
(42) Kruse, P. W. *Proc. SPIE* **2004**, *5406*, 437.
(43) Coath, J. A.; Richardson, M. A. *Proc. SPIE* **1999**, *3738*, 555.
(44) Kats, M. A.; Sharma, D.; Lin, J.; Genevet, P.; Blanchard, R.; Yang, Z.; Qazilbash, M. M.; Basov, D. N.; Ramanathan, S.; Capasso, F. *Appl. Phys. Lett.* **2012**, *101*, 221101.
(45) Cao, J.; Fan, W.; Zhou, Q.; Sheu, E.; Liu, A.; Barrett, C.; Wu, J. *J. Appl. Phys.* **2010**, *108*, 083538.
(46) Rúa, A.; Fernández, F. E.; Sepúlveda, N. *J. Appl. Phys.* **2010**, *107*, 074506.
(47) Wang, K. X.; Cheng, C.; Cardona, E.; Guan, J. Y.; Liu, K.; Wu, J. *ACS Nano* **2013**, DOI: 10.1021/nn305419e.
(48) Mirfakhrai, T.; Madden, J. D. W.; Baughman, R. H. *Mater. Today* **2007**, *10*, 30.
(49) Liu, K.; Fu, D. Y.; Cao, J.; Suh, J.; Wang, K. X.; Cheng, C.; Ogletree, D. F.; Guo, H.; Sengupta, S.; Khan, A.; Yeung, C. W.; Salahuddin, S.; Deshmukh, M. M.; Wu, J. *Nano Lett.* **2012**, *12*, 6272.
(50) Nakano, M.; Shibuya, K.; Okuyama, D.; Hatano, T.; Ono, S.; Kawasaki, M.; Iwasa, Y.; Tokura, Y. *Nature* **2012**, *487*, 459.

Supporting Information for

Axially Engineered Metal-Insulator Phase Transition by Graded Doping VO_2 Nanowires

Sangwook Lee, Chun Cheng, Hua Guo, Kedar Hippalgaonkar, Kevin Wang, Joonki Suh, Kai Liu and Junqiao Wu

1. Device fabrication for electrical measurements free of strain.

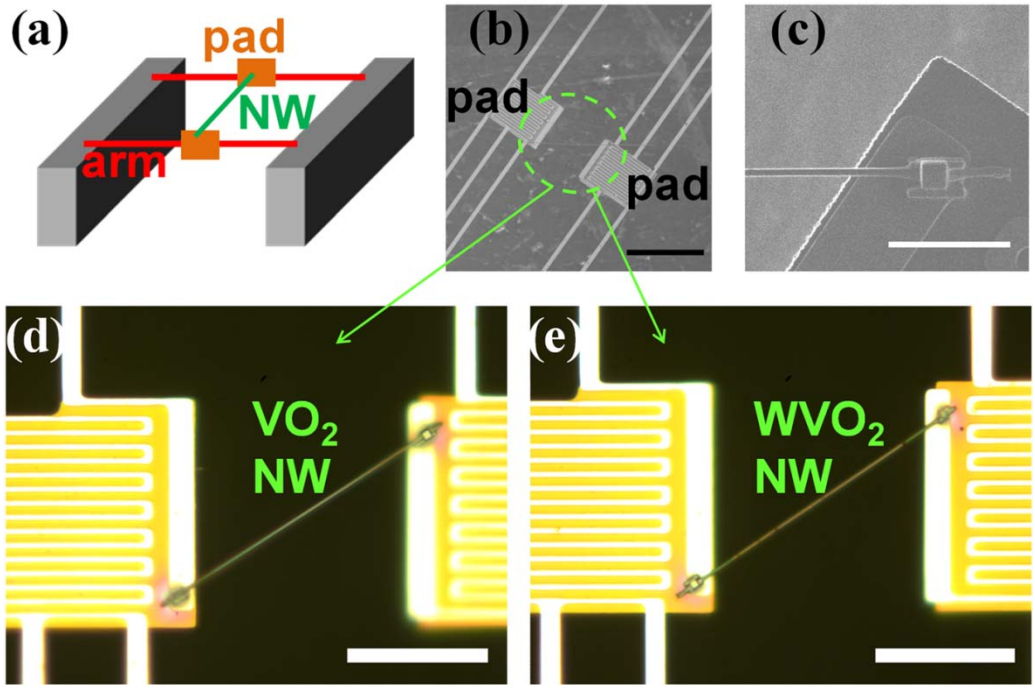

Figure S1. *Suspended pad based microdevice used for electrical measurements. Scheme of the device structure (a), SEM images showing the top view of the device (b), FIB-deposited Pt/C composite to bond the NW onto the pad (c), and optical images of the fabricated devices with an undoped VO_2 NW (d) and a graded doped WVO_2 NW (e). Scale bars: 50 μm (b), 5 μm (c), 20 μm (d), 20 μm (e).*

2**. Close-up optical image of a root-cantilevered NW as a micro-thermometer.**

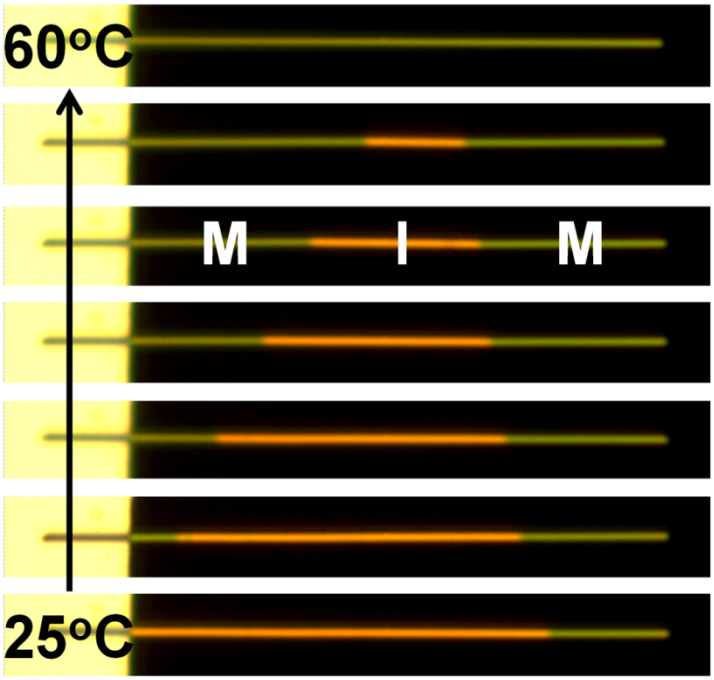

Figure S2*. Progressive M domain growth with increasing temperature in a graded doped WVO_2 NW. The wire length is ~35 μm.*

3. Length shrinkage of a WVO_2 NW: the basis for micro-actuation.

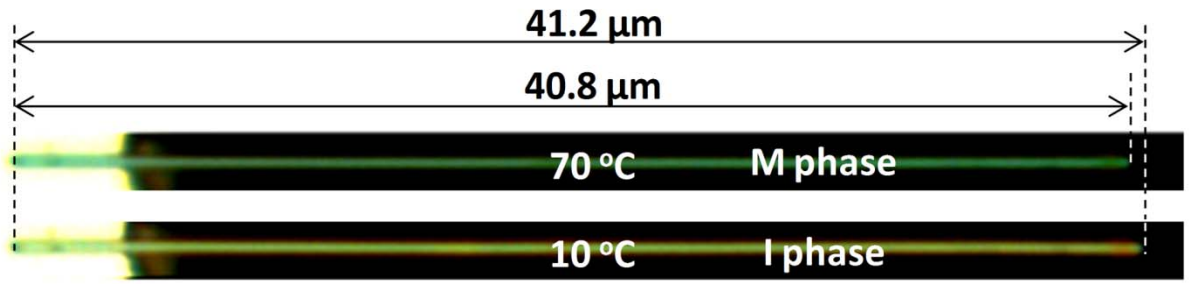

Figure S3*. Optical images showing length change by complete phase transition of a graded doped WVO_2 NW. The overall length decreases by ~ 1% between the M and the I phases.*

4. Suggested mechanism for the axially graded doping of W in VO_2 NWs.

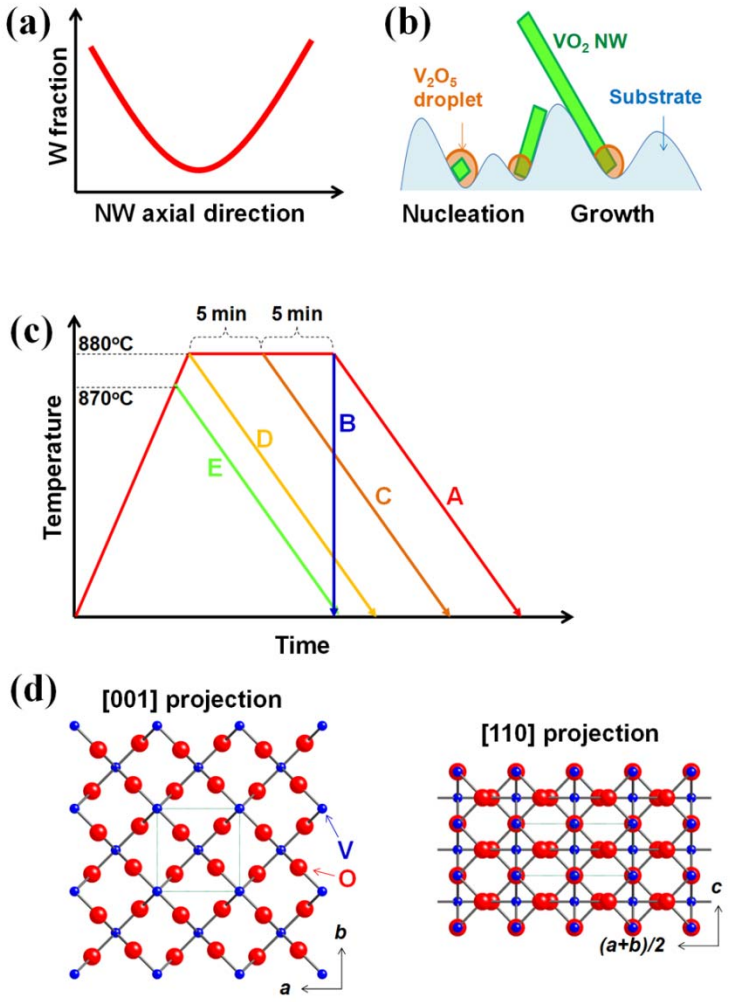

Figure S4. *(a) A sketch showing the typical W fraction along the graded W-doped VO_2 NW. (b) Mechanism of growing free-standing VO_2 NWs on rough quartz substrates using V_2O_5 powder as the source.* [S1] *At the growth temperature when VO_2 nucleates and grows out of the V_2O_5 droplet, owing to capillary force, the VO_2 NWs are initially bound onto the local substrate surface. However, at later times, following the surface roughness, the NWs grow out of the surface plane and become free-standing. (c) A schematic showing various temperature profiles we tried for the NW synthesis. (d) The structural model of the VO_2 rutile (M phase); [001] projection (viewed along the c_R axis), and [110] projection.*

Our graded doped WVO_2 NWs show "V"-shape W doping profile along the axial direction, as sketched in **Fig. S4a**. The mechanism of axially graded doping of W in the VO_2 NWs is not fully understood, but an explanation is given below.

First, we note that these NWs were grown catalyst-free, [S2] and the rough geometry of substrate surface is exploited to facilitate the growth of free-standing NWs, as shown schematically in **Fig. S4b**.[S1] Otherwise, most of the NWs are grown firmly clamped onto, or half-embedded into the surface, imposing large strain to the NWs and influencing their MIT behavior. [S2] Liberating the NWs from the substrate by chemical etch is possible, but gives low yield and may damage the surface of the NWs.

Secondly, in **Fig. S4c** we show a few possible temperature profiles we tried for the growth. In route B, the sample was taken out of the tube furnace abruptly (within ~ seconds) after the 880^{o}C growth. In all other routes, the temperature ramping up and down processes were on the order of 50^{o}C/min, and were controlled by the temperature controller of the furnace. We observed that i) No NWs were grown at all in route E; ii) NWs were grown in route A, B, C and D, and surprisingly they all yielded NWs with similar lengths; iii) all A, B, C and D growths led to "V"-shape W doping in VO_2 NWs; and iv) the average W doping levels were the highest for route A and the lowest for D.

We now discuss two possible W doping mechanisms: W incorporation during the NW growth, and W doping by axial diffusion after the NW growth.

1) W incorporation during the NW growth. In this picture, the W atoms are incorporated into the VO_2 NW while the NW is forming. Because WO_2 has different vapor pressure from that of V_2O_5, it is possible that W incorporation is more efficient at relative low temperatures slightly below 880^{o}C. In this way both the root and the tip of the VO_2 NW were heavily doped with W, because they are the parts of the NW that formed at slightly lower temperatures (i.e., during the temperature ramping up and ramping down processes).

However, our observation iii above shows that the NWs were still doped as the "V"-shape W profile even in absence of the temperature ramping down process (route B). This is contradicting with the idea that W atoms were incorporated during the NW formation. This idea is also inconsistent with the observation ii. We therefore propose:

2) W doping by axial diffusion after the NW formation. In this picture, the VO_2 NWs were rapidly grown, and then W diffuses along the axis of the NW from the two ends towards the center, fed by the W vapor and assisted by the high temperature.

This is consistent with all the observations above. V_2O_5 micro-droplets are transported to the substrate at high temperatures, and an un-doped VO_2 NW rapidly forms from each liquid V_2O_5 droplet when temperature approaches 880^{o}C. This NW stops to grow when its V_2O_5 droplet is depleted even if the V_2O_5 vapor supply continues; therefore, longer growth time at 880^{o}C (from routes D to C to A) does not grow longer NWs. The formation of VO_2 NW is too fast for significant amount of W to be doped in, therefore, these rapidly formed VO_2 NWs are nominally un-doped or only lightly doped. Instead, W atoms axially diffuse from the two ends of each already-grown VO_2 NW toward the center, resulting in a "V"-shape W doping profile. This diffusion process is fed by the abundant W vapor and assisted by the high temperature of the furnace. The diffusion is mostly axial instead of radial along the NWs because of diffusion anisotropy. The high-temperature crystal structure (rutile phase) of the VO_2 NWs has large openings along the NW axis (c_R) direction acting as diffusion channels for the W atoms, but the V and O atoms are much more closely packed in the NW radial direction (i.e., directions perpendicular to c_R) (**Fig.S4d**); this allows a much easier axial diffusion than radial diffusion. In TiO_2 which has a similar rutile structure, it has been reported that some cations diffuse more easily along the c-direction channels.[S3-S5] Such quasi-one-dimensional diffusion warrants further investigation and may be used to achieve other novel structures.

References

(S1) Cheng, C.; Liu, K.; Xiang, B.; Suh, J.; Wu, *J. Appl. Phys. Lett.* **2012**, *100*, 103111.

(S2) Wu, J.; Gu, Q.; Guiton, B. S.; de Leon, N. P.; Ouyang, L.; Park, H. *Nano Lett.* **2006**, *6*, 2313.

(S3) Van Orman, J. A.; Crispin, K. L. *Rev. Mineral. Geochem.* **2010**, *72*, 757.

(S4) Johnson, O. W. *Phys. Rev.* **1964**, *136*, A284.

(S5) Steele, J. L.; Mccartney, E. R. *Nature* **1969**, *222*, 79.